Electrically and Optically Tunable Plasmonic Guest–Host Liquid Crystals with Long-Range Ordered Nanoparticles

Qingkun Liu,[†] Ye Yuan,[†] and Ivan I. Smalyukh*,[†,‡,§]

[†]Department of Physics and [‡]Department of Electrical, Computer, and Energy Engineering, Materials Science and Engineering Program, and Liquid Crystal Materials Research Center, University of Colorado, Boulder, Colorado 80309, United States

[§]Renewable and Sustainable Energy Institute, National Renewable Energy Laboratory and University of Colorado, Boulder, Colorado 80309, United States

S Supporting Information

ABSTRACT: Practical guest–host devices in which dichroic dye molecules follow electrical switching of a liquid crystal host remain elusive for decades despite promising efficient displays and emergent applications such as smart windows. This is mainly because of poor stability, surface precipitation, and limited means for property engineering of the dyes. To overcome these challenges, we develop plasmonic metal nanoparticle analogues of dichroic guest–host liquid crystals. Nematic dispersions of aligned anisotropic gold nanoparticles are obtained by polymer passivation of their surfaces to impose weak tangential boundary conditions for orientation of anisotropic host molecules. Control of the ensuing surface interactions leads to long-range ordered colloidal dispersions, allowing for collective optical and electrical switching of rod- and platelet-like nanoparticles. This facile control of mesostructured plasmonic medium's optical properties in visible and infrared spectral ranges is of interest for many applications.

KEYWORDS: Liquid crystal, gold nanoparticles, plasmonic, guest–host display, self-assembly
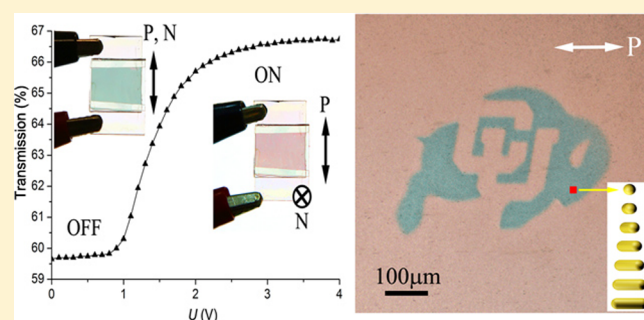
Macroscopic behavior of materials begins to manifest itself at the mesoscale at which control of structure and composition is the emergence of engineering previously unrealized material functionality.[1,2] Self-assembly of functional nanounits, such as quantum dots, plasmonic, magnetic, and core–shell colloids, is an exceptionally promising approach to the design and scalable fabrication of these mesostructured materials.[2–4] Furthermore, ordered assemblies of nanoparticles in liquid crystals (LCs) may enable composites with properties that can be tuned by fields, light, and other external stimuli.[4–10] This may lead to cheaper and more efficient technology as well as a fertile ground for new fundamental science. However, practical realization of such tunable mesoscale LC composites is hindered by poor nanoparticle dispersion. Spontaneous alignment of dichroic and fluorescent dye molecules in LCs, which results from anisotropic molecular-scale interactions, is widely used in imaging of orientational ordering, defects, and structures,[11] as well as in "guest–host" devices.[12,13] On the other hand, being much larger than molecules, microparticles locally distort the nematic alignment and induce topological defects,[1,6–9] leading to assemblies that minimize their free energy cost.[9] However, at mesoscopic scales between the size of molecules and hundreds of nanometers, behavior of solid inclusions in LCs is poorly understood and rarely controlled[4,5] as they tend to aggregate. This is due to poorly controlled particle-induced elastic distortions that result in elasticity-

mediated forces leading to minimization of the elastic free energy through "sharing" of distortions produced by different individual nanoparticles. Orientational switching of anisotropic nanoparticles in concentrated dispersions is also a challenge.[5]

In this Letter, we develop long-range ordered LC dispersions of anisotropic colloids, such as gold nanoparticles (GNPs) with facile response to low-voltage fields and low-intensity light. Nematic dispersions of gold nanoparticles are obtained by polymer passivation of their surfaces to impose weak tangential boundary conditions for orientation of anisotropic host LC molecules. This allows us to mitigate elastic distortions imposed by surface boundary conditions on these nanoparticles, so that no additional elasticity-mediated interactions emerge[9] and polymer stabilization of GNPs works well not only in isotropic but also in mesomorphic phases of the LC hosts. Similar to dichroic dye molecules in the guest–host LCs and Heilmeier displays,[12,13] the GNPs follow switching of the director **N** describing average local LC molecular orientations. We quantitatively explain how this behavior arises from anisotropic surface interactions and leads to strong polarization-sensitive and voltage- or light-tunable surface plasmon resonance (SPR) effects. Our findings may enable composite
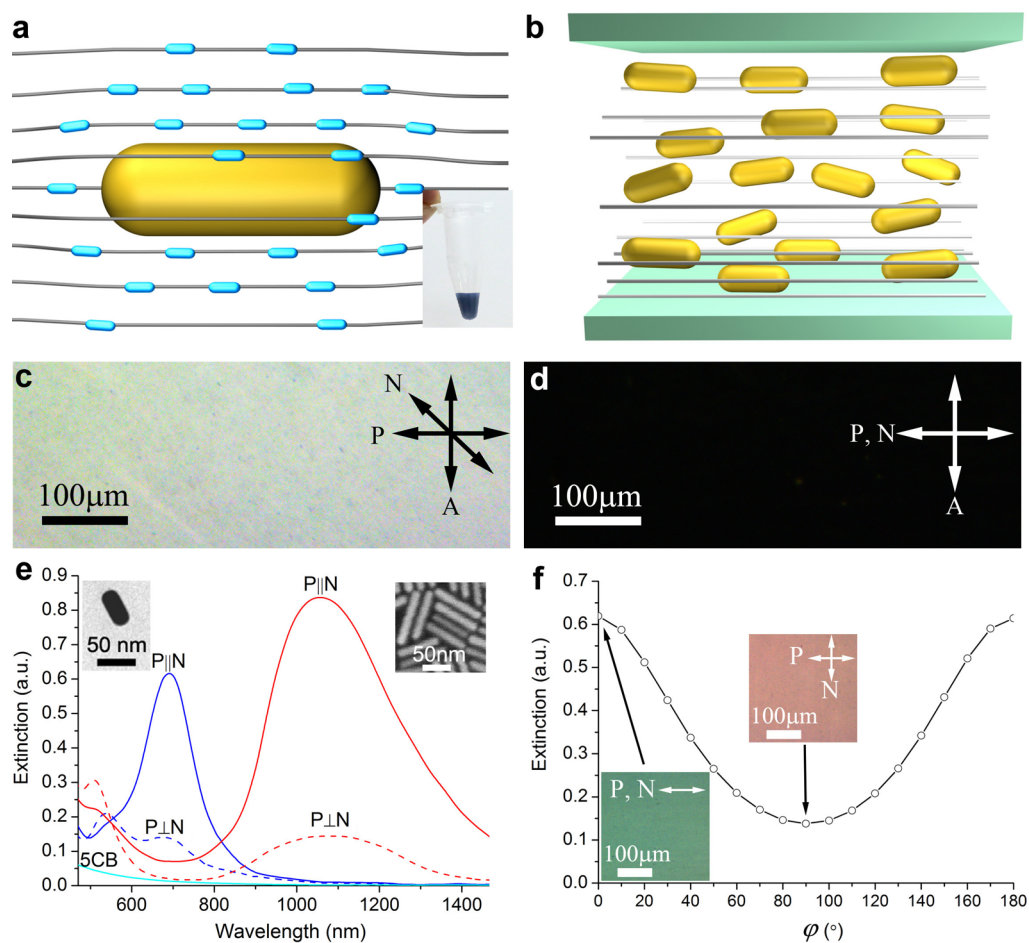
Figure 1. Alignment of gold nanorods in a nematic LC. (a) Schematic of a nanorod with weak tangential boundary conditions for (cyan) rodlike LC molecules. The inset shows a vial with the GNP-5CB dispersion. (b) Schematic of dispersed nanorods following **N**. (c,d) POM micrographs of the GNP-LC composite with **N** at (c) 45° and (d) 0° to **P**. (e) Extinction spectra of aligned short (blue curves) and long (red curves) gold nanorods in a nematic host for **N** parallel and perpendicular to **P** with the spectrum of pure 5CB (cyan curve) shown for reference. The insets of (e) show a TEM image of a short nanorod and an SEM image of longer nanorods. (f) Extinction of short gold nanorods at longitudinal SPR peak versus φ.

materials with tunable properties emerging from combining switchable nanostructures of anisotropic fluids with SPR and other properties of anisotropic nanoparticles as well as a new generation of guest−host LC displays.

Aqueous dispersions of gold nanorods with mean diameters and lengths of 20 × 50 nm were synthesized by following ref 14 and the 14 × 88 nm nanorods were synthesized using the method of ref 15. Triangular nanoplatelets with a mean lateral size of 50 nm and thickness of 13 nm were synthesized using a galvanic replacement method.[16] These methods of synthesis are described in detail in the Supporting Information. The dispersions were centrifuged at 9000 rpm for 20 min twice and then resuspended into deionized water to remove cetyltrimethylammonium bromide used in synthesis. To disperse in LCs and weaken interactions between the director **N** and nanoparticle surfaces,[17] we functionalized GNPs by thiol-terminated methoxy-poly(ethylene glycol) (mPEG-SH, JemKem Technology).[18] For this, 1 mL of aqueous solution with 30 mg of 5 kDa mPEG-SH was added to 50 mL of a diluted GNP dispersion with optical density of 4. After sitting for 24 h, this dispersion was purified via centrifugation to eliminate the excess mPEG-SH. The recapping was repeated twice to fully coat GNP surfaces with mPEG. The GNPs were then transferred into methanol via centrifuging at 9000 rpm for 20 min and washing by methanol three times. Full evaporation

of the solvent from 50 μL of GNP dispersion in 0.5 mL centrifuge tube within 1 h at 90 °C was followed by adding 15 μL of a nematic 4-cyano-4′-pentylbiphenyl (5CB, Chengzhi Yonghua Display Materials Co. Ltd.). The mixture was sonicated for 5 min at 40 °C, yielding an excellent dispersion in the isotropic phase of 5CB, which was cooled down to the nematic phase while vigorously stirring. This procedure mitigated aggregation caused by isotropic-nematic front propagation and nucleation of nematic domains within the isotropic melt and is a critically important element of preparation of stable colloidal dispersions of nanoparticles in LCs.[19] The ensuing composites were then centrifuged at 3000 rpm for 5 min to remove residual aggregates, so that the final LC dispersion contained only individual GNPs.

LC cells were fabricated from glass plates coated with transparent indium tin oxide electrodes on their inner surfaces, which were rubbed to impose boundary conditions for **N** and glued together with UV-curable NOA-65 glue (Norland Products, Inc.) containing 5−60 μm silica spacers to define the desired cell gap. The actual local thickness of the LC cell was measured by an optical interference method using microspectroscopy and was found to be within ±0.5 μm of that defined by the silica spacers.[20] Photoalignment layers were obtained by spin-coating azobenzene polymer PAAD-22 (BEAM Co.) at 3000 rpm for 60 s and baking at 100 °C for
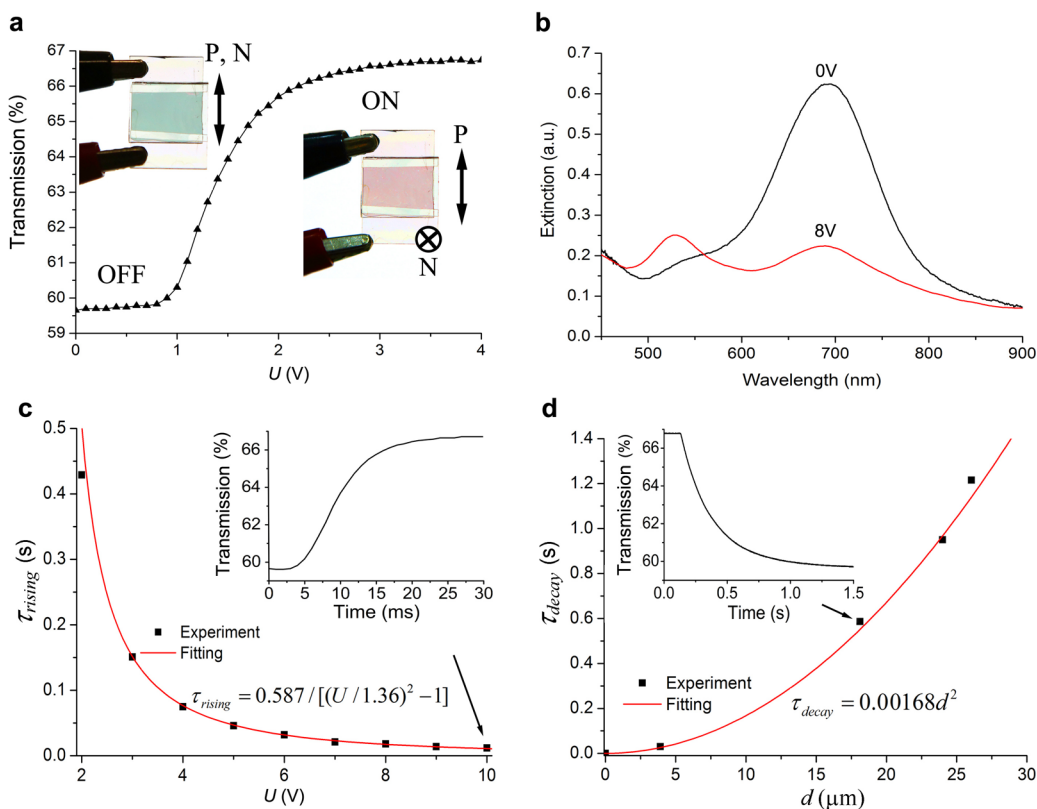
Figure 2. Electric switching of plasmonic guest−host LCs with short gold nanorods. (a) Transmission versus voltage U. Insets show the corresponding color change. (b) Voltage-dependent extinction spectra for **P** along the rubbing direction. (c) Rising time versus U obtained from transmission versus time curves, such as the one shown in the inset for $d = 18$ μm and $U = 10$ V. (d) Decay time versus d obtained from transmission versus time curves, such as the one shown in the inset for $d = 18$ μm. The fitting formulas are shown near the red fitting curves in (c,d).

10 min.[21] Polarized blue light illumination of power ∼50 μW for 5 min set boundary conditions for **N** to be perpendicular to its linear polarization. This alignment persisted under ambient and imaging light but could be controlled by varying polarization of spatially patterned blue-light illumination controlled on a pixel-by-pixel basis using a LC microdisplay with 1024 × 768 pixels (EMP-730, Epson) coupled to an upright optical microscope.[22]

Optical imaging of composites was performed using an Olympus BX-51 polarizing optical microscope (POM) equipped with 10× , 20× , and 50× air objectives (all from Olympus) with numerical aperture NA = 0.3−0.9 and a CCD camera (Spot 14.2 Color Mosaic, Diagnostic Instruments, Inc.). Polarized extinction spectra were probed using a microscope-mounted spectrometer USB2000-FLG (Ocean Optics) or an optical spectrum analyzer HP70951A (Agilent Technologies, Inc.) by detecting achromatic light from an Integrating Sampling System (ISS-2, Ocean Optics) passing through the LC cell and a rotatable polarizer. Dark-field optical microscopy utilized an oil-immersion dark-field condenser (NA = 1.2), so that only highly scattered light was collected using a 20× objective and passed to a CCD camera through a rotatable polarizer. The electro-optic response of GNP-LC composites was characterized by use of a multifunction data acquisition system SCC-68 (National Instruments Co.) controlled by homemade software written in Labview (National Instruments Co.) and a Si amplified photodetector PDA100A (Thorlabs Inc.). Band-pass optical interference filters of 693.5−706.5 nm and 651−671 nm (both from Semrock Inc.) were used to selectively probe switching of short gold nanorods (20 × 50

nm) and nanoplates in LC in the vicinity of their longitudinal and in-plane SPR wavelengths, respectively.

In a 5CB nematic LC host medium, longitudinal SPR peaks of our short and long nanorods shift to 690 and 1080 nm, respectively, because of the medium's higher refractive index compared to water (Supporting Information Figure S1). Behaving like "guest" dye molecules in the LC "host",[12] dispersed nanorods follow the director **N** controlled on centimeter scales via surface rubbing or polarized illumination of photoalignment layers (Figure 1a−d and Supporting Information Figure S2). Owing to the shape anisotropy, the longitudinal and transverse SPRs differ from each other, so that extinction spectra of the aligned nanorod-LC dispersion depend on the linear polarization **P** of excitation light (Figure 1e). For **P**‖**N**, the longitudinal SPR of short nanorods is excited, so that the composite appears green. For **P**⊥**N**, mostly only the transverse SPR is excited, causing the red-color appearance. The orientational scalar order parameter of nanorods can be determined from extinction spectra as $S = (A_\parallel − A_\perp)/(A_\parallel + 2A_\perp)$,[12] where $A_\parallel$ and $A_\perp$ are peak extinctions of longitudinal SPR for **P**‖**N** and **P**⊥**N**, respectively. We obtain $S = 0.537$ for short and $S = 0.610$ for longer nanorods (Figure 1e). The extinction of short gold nanorods (20 × 50 nm) at longitudinal SPR peak versus angle φ between **N** and **P** follows the expected ∝$\cos^2 \varphi$ dependence (Figure 1f).

Electric alignment of particles in isotropic fluids requires voltages of $10^2 - 10^5$ V,[23−25] impeding practical applications such as displays. However, mediated by the host, LC-dispersed GNPs collectively rotate with **N** at voltages as low as 1 V. To probe this switching, the composites of short gold nanorods
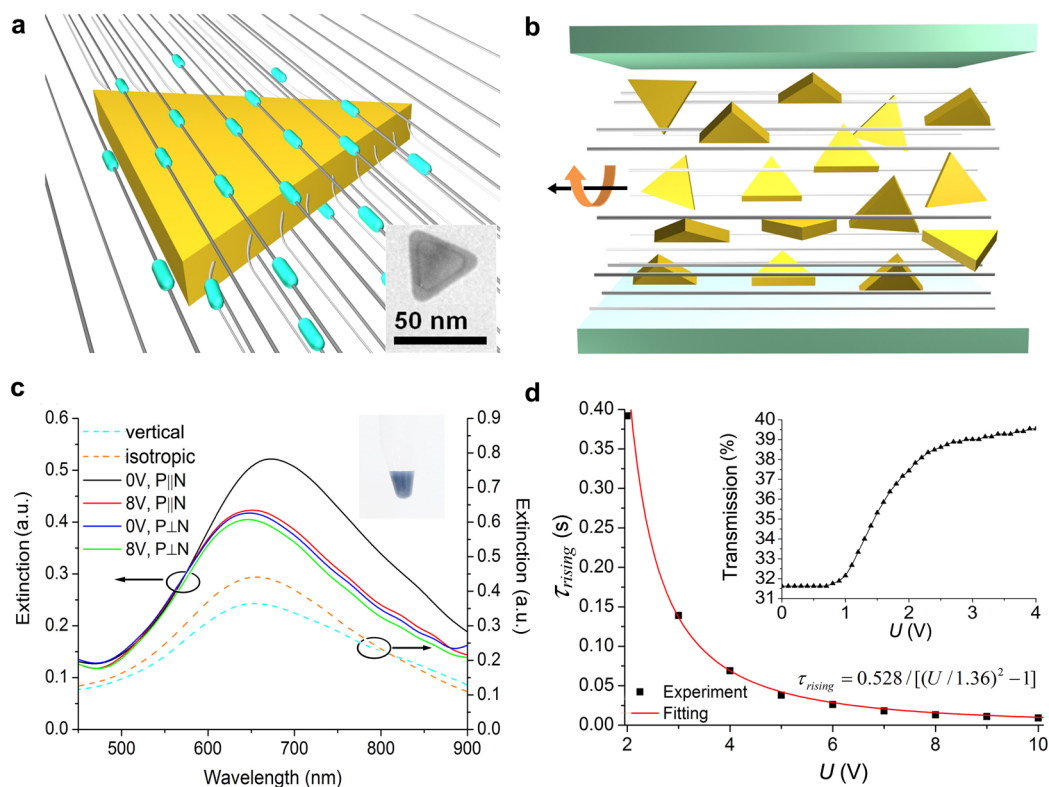
Figure 3. Plasmonic guest−host LCs with aligned nanoplatelets. (a) Schematic of a platelet with tangential boundary conditions for (cyan) LC molecules with the inset showing its TEM image. (b) Schematic of dispersion with platelet normals aligned, on average, orthogonally to **N**. (c) Polarized-light extinction spectra for different voltages and angles (solid curves) and unpolarized-light extinction spectra for vertical **N** and in an isotropic phase (dashed curves). (d) Rising time versus U and the corresponding theoretical fit. The inset shows a typical transmission versus U dependence.

(20 × 50 nm) in 5CB are infiltrated into planar cells. After passing through a polarizer, white incident light has electric field **E** oscillating along **N** and exciting the longitudinal SPR (Figure 2a,b), so that the cell appears green (Figure 2a). The 5CB has a positive dielectric anisotropy $\Delta\varepsilon = \varepsilon_{\parallel} - \varepsilon_{\perp} = 9$, where $\varepsilon_{\parallel}$ and $\varepsilon_{\perp}$ are dielectric constants measured for fields parallel and perpendicular to **N**, respectively. Thus, at high voltages, **N** and rods rotate to become vertical, so that the transverse SPR is excited (Figure 2b) and the cell appears red (Figure 2a). The small bump at longitudinal SPR peak at 8 V arises due to the order parameter of GNPs in the LC host being $S = 0.537 < 1$, which implies gold nanorods could not orient perfectly along the electric field. Another reason is that both the LC director and gold nanorods near the confining surfaces do not fully reorient in electric field even at relatively high voltages such as 8 V because of the planar surface boundary conditions on the LC director imposed by alignment layers. This resembles the behavior of dichroic-dye-based guest−host LCs in which dichroic dyes also exhibit scalar order parameter $S < 1$ and also show incomplete realignment in near-surface regions of planar cells due to the action of boundary conditions.[12] Although GNPs at used concentrations can slightly modify LC properties, the ∼1 V realignment threshold of our composite is close to $U_{\text{th}} = \pi[K_{11}/(\varepsilon_0\Delta\varepsilon)]^{1/2}$ of pristine 5CB,[26] where $\varepsilon_0 = 8.854 \times 10^{-12}$ C V^{-1} m^{-1} and splay elastic constant $K_{11} = 5.4$ pN.[27]

Dynamics of electrical switching of short gold nanorods in LC is probed using bandpass filters matching the longitudinal SPR peaks. Rising and decay times are deduced from transmitted intensity changes between 10 and 90% and

compared to the theoretical prediction for pristine and guest−host LCs $\tau_{\text{rising}} = \tau_{\text{decay}}/[(U/U_{\text{th}})^2 - 1]$,[26] where $\tau_{\text{decay}} = \gamma_1 d^2/(K_{11}\pi^2)$ is the decay time, γ_1 is the rotational viscosity, and d is the cell thickness. Taking $\gamma_1 = 0.0806$ Pas for pristine 5CB measured in literature,[28] we obtain the ratio $\gamma_1/(K_{11}\pi^2) = 1.5 \times 10^{-3}$ s/μm^2 expected for the pristine LC. The rising time of the GNP-LC composite shows the same voltage dependence as the LC host (Figure 2c). The measured decay time of switching the GNP-LC composite increases with cell thickness as $\propto d^2$ (Figure 2d). Fitting the experimental curve gives $\gamma_1/(K_{11}\pi^2) = 1.68 \times 10^{-3}$ s/μm^2, which is slightly larger than that of pristine 5CB. This finding is natural as addition of gold nanorods, which are much bigger than the LC molecules, is expected to increase the effective viscosity of the composite medium as compared to the pristine LC. Additionally, because the response times are characterized by passing light over a cell region of diameter ∼2 mm, the experiment might be somewhat influenced by the ±0.5 μm nonuniformity of the LC cell thickness. Finally, the response might be further influenced by secondary effects such as small lagging in the rotational response of nanoparticles as compared to that of the LC director to which they are mechanically coupled, redistribution of GNPs across the cell thickness upon switching and changing amplitude of the applied electric field due to the anisotropic dielectrophoretic effects or due to the influence of field-induced elastic distortions across the cell thickness, and so forth. Despite such a large number of factors that could be influencing the dynamics of the plasmonic LC composite switching, which will be explored in details elsewhere, we find it remarkably close to that of pristine LCs and dichroic-dye-based LCs, especially if
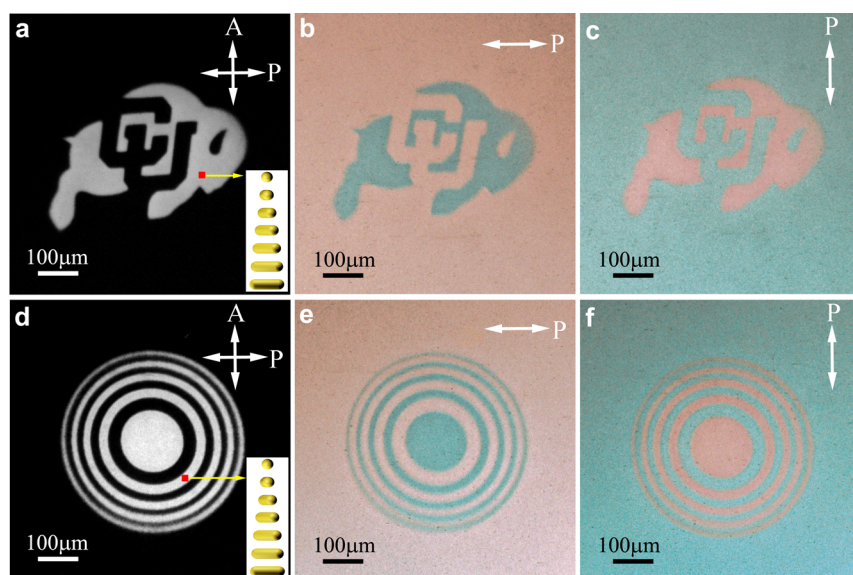
Figure 4. Optical realignment and patterning of plasmonic guest−host LCs. (a) A POM micrograph of a "buffalo"-shaped twist domain in a uniformly aligned cell obtained by patterned illumination of the photoalignment layer. (b,c) The corresponding bright-field micrographs for polarizations of incident light (b) perpendicular and (c) parallel to **N**. (d) POM and (e,f) bright-field micrographs of a Fresnel zone plate created by patterned illumination. Insets in (a,d) depict the $\pi/2$-twist of **N** and nanorods across the cell thickness within twist domains.

accounting for an increased effective viscosity of the composite as compared to pure 5CB (Figure 2).

In addition to nanorods, LCs can orientationally order anisotropic GNPs with other geometric shapes. To demonstrate this, we use polygonal nanoplatelets that tend to align with their large-area faces parallel to **N** while freely rotating around it (Figure 3). The normals of nanoplatelets point, on average, perpendicular to **N** and undergo rotational thermal fluctuations (Figure 3a,b), consistent with experimental polarization-dependent extinction spectra of used equilateral triangular nanoplatelets with dimensions of 50×13 nm (Figure 3c). Prior theoretical studies[29] of the polarized in-plane and out-of-plane SPR modes of metallic nanoplatelets allow us to interpret our findings as follows. The in-plane SPR mode is excited when polarization of light is parallel to nanoplatelets, exhibiting a red-shifted extinction peak at around 680 nm. The out-of-plane SPR mode is excited when this polarization is orthogonal to platelets, showing a much smaller blue-shifted extinction peak. Because of the achieved orientational ordering with normals of nanoplatelets pointing, on average, perpendicular to **N** (and large-area platelet faces parallel to **N**) one observes mainly only the in-plane SPR for **P**∥**N** and an average of in-plane and out-of-plane modes for **P**⊥**N**. This is a plasmonic analogue of dichroic guest−host LCs with disclike dye molecules aligning with their normals, on average, perpendicular to **N**. A scalar order parameter describing orientational ordering of normals to gold nanoplatelets is $S = 2(A_V/A_I - 1) \approx -0.350$, where A_V and A_I are unpolarized-light extinctions measured for platelets in cells with vertical **N** and after melting the LC to isotropic phase at 45 °C, respectively (Figure 3c).[30] Because $S = -0.350 > -0.5$, contributions of both in-plane and out-of-plane modes are present for both orientations of the linear polarization of excitation light. To keep the polar surface anchoring free energy at minimum, nanoplatelets also follow electrical switching of **N** with the observed realignment threshold and switching dynamics similar to those of pristine and nanorod-doped LCs (Figure 3d).

In addition to fields and surface rubbing, GNP dispersions can be aligned and controlled by light (Figure 4 and Supporting Information Figure S3). Photoalignment layers define the surface boundary conditions for **N** parallel to their azobenzene groups that orient orthogonally to the linear polarization of the patterning blue light illumination. This allows one to first align the composite unidirectionally and then induce $\pi/2$-twist domains with GNPs following **N**, as guided by polarized illumination patterns. In our cells, light propagation within twist domains satisfies the so-called Mauguin condition,[12] so that traversing light's linear polarization direction also follows rotation of **N**. Therefore, longitudinal and transverse SPRs of aligned nanorods can be excited selectively, as determined by mutual orientations of **N** and the linear polarization of incident light (Figure 4). When viewed in polarized white light, the twisted and nontwisted areas exhibit different colors due to selective excitation of SPR modes. As demonstrated using an example of short 20×50 nm nanorods, anisotropic GNP orientations and perceived colors can be tuned dynamically through defining boundary conditions at one or both confining plates (Figure 4).

Polymer-based stabilization of colloidal GNP dispersions is well-known and was achieved previously in different isotropic solvents, including both polar and nonpolar fluid media,[14−16,23−25] and is effective when dispersing nano-inclusions in isotropic melts of LCs. The biggest challenge in achieving a similar dispersion in thermotropic LCs arises from the fact that these nanoparticles induce distortions of the LC director field, which cost elastic free energy and therefore promote aggregation. This aggregation of nanoparticles with strong surface boundary conditions allows the LC to reduce the overall free energy due to such distortions induced by individual interacting particles, because multiple particles can "share" these elastic distortions. By realizing polymer capping with weak tangentially degenerate surface anchoring, we were able to eliminate the particle-induced director distortions and, thus, also the attractive elasticity-mediated interactions between the nanoparticles. Because of their geometrically anisotropic

shapes, interactions of the nanoparticles with the anisotropic host fluid in this case are driven solely by surface anchoring energy minimization, which results in their alignment with respect to the uniform far-field director. Weak tangentially degenerate surface boundary conditions through polymer passivation of solid surfaces were previously achieved only on flat glass surfaces[17] but not on curved surfaces of nanoparticle. Our demonstration of feasibility of achieving this on curved nanoparticle surfaces, along with the fact that it allows for colloidal stability and orientationally ordered dispersion in mesomorphic fluid hosts, may allow for extending our approach to other types of metal, dielectric, and semiconductor nanoparticles, as long as proper surface functionalization by polymer chains can be achieved.

We built a physical model to further explain the excellent dispersion and long-range alignment of anisotropic GNPs controlled by weak surface interactions due to varying relative orientations of the uniform **N** and LC-GNP interfaces with weak tangentially degenerated boundary conditions. Because our GNPs are smaller than the surface anchoring extrapolation length $l_e = 100-1000$ nm, the director couples only weakly to GNP surfaces,[26] so that elastic colloidal interactions can be neglected indeed.[9,31−33] Because of tangential boundary conditions, the surface anchoring energy is minimized when long axes of nanorods align along **N**, although thermal fluctuations tend to randomize their orientations. Assuming the Rapini−Papoular form of the surface anchoring potential, $f_{sa} = (W/2)\sin^2 \beta$ where β is an angle between **N** and nanorod's surface,[32] we find the total surface free energy by integrating f_{sa} over the GNP surface. The equilibrium distribution of nanorod orientations due to these interactions follows Boltzmann statistics $f_s(\theta) \propto \exp(-\delta \sin^2 \theta)$, where θ is the angle between **N** and a long axis of a nanorod with length L and radius R, $\delta = \pi LRW/(2k_BT)$, where k_B is Boltzmann constant, and $T \approx 300$ K is the absolute temperature. The orientational order parameter can be found as[26]

$$S = \int_0^\pi P_2(\cos \theta) f_s(\theta) \sin \theta \, d\theta \qquad (1)$$

yielding $S = 3 \exp(\delta)/[2(\pi\delta)^{1/2}\text{Erf}(i\sqrt{\delta})/i] - 3/(4\delta) - 1/2$, where $\text{Erf}(x)$ is the error function defined as $\text{Erf}(x) = 2/\sqrt{\pi}\int_0^x e^{-t^2} \, dt$. Applying this model to both short ($L \approx 50$ nm, $R \approx 10$ nm) and longer ($L \approx 88$ nm, $R \approx 7$ nm) nanorods that exhibit experimentally measured order parameters $S = 0.537$ and $S = 0.610$, respectively, we deduce the same values of the polar anchoring coefficient $W = (1.95 \pm 0.06) \times 10^{-5}$ J/m^2.

The mechanism of aligning gold nanoplatelets is similar to that of gold nanorods, which arises from the weak planar surface anchoring of LC molecules by the polymer on nanoplatelets' surfaces. Due to tangentially degenerate boundary conditions, the polar surface anchoring energy is minimized when platelets align with their large-area faces parallel to the far-field director. The competition between these anisotropic surface anchoring interactions and thermal fluctuations results in the observed alignment with the normals of nanoplatelets pointing, on average, perpendicular to the LC's director and undergoing rotational thermal fluctuations (Figure 3). For nanoplatelets of lateral size D, the distribution of orientations is $f_s(\psi) \propto \exp(-\xi \cos^2\psi)$, where $\xi = \sqrt{3}D^2W/(4k_BT)$ and ψ is the angle between **N** and the platelet normal. Using eq 1, we find $S = -3 \exp(-\xi)/[2(\pi\xi)^{1/2}\text{Erf}(\sqrt{\xi})]+3/(4\delta) - 1/2$. Taking $W = 1.95 \times 10^{-5}$ J/m^2 and $D = 50$ nm, we

obtain S=-0.355, consistent with the order parameter found from the experimental polarization-dependent extinction spectra shown in Figure 3c. The measured and calculated values of S for the estimated polar anchoring coefficient $W = 1.95 \times 10^{-5}$ J/m^2 for different nanoparticles are listed in Table 1, demonstrating a very good agreement with each other and confirming our explanation of dispersion and alignment of GNPs in the LC host.

Table 1. Measured and Calculated Values of S for $W = 1.95 \times 10^{-5}$ J/m^2

	short gold nanorods	long gold nanorods	nanoplatelets
calculated S	0.524	0.610	−0.355
measured S	0.537	0.610	−0.350

To conclude, we have developed plasmonic guest−host LCs that can be engineered for switching of material properties and light propagation in both visible and infrared spectral ranges. This ordered dispersion of anisotropic metal nanoparticles in nematic hosts is enabled by controlled weak anisotropic interactions between their surfaces and the LC host. Potential applications include the design of novel hybrid nanostructured materials and self-assembly based fabrication of electro-optic and all-optical devices, such as tunable nanoantennae, plasmonic diffraction components, smart windows, switchable plasmonic polarizers, and so forth. By properly choosing terminal groups of mPEG or similar polymers, our method can be applied to nanoparticles with other shapes and composition, such as quantum dots, magnetic and up-conversion nanoparticles, and so forth. This in turn may lead to a broad range of mesostructured composite materials with tunable pre-engineered properties and many applications. Our ordered dispersions of anisotropic particles may also give rise to fundamentally new mesophases with low symmetry and new composite properties.

■ ASSOCIATED CONTENT

Ⓢ Supporting Information

Details of synthetic condition of nanoparticles and sample characterization including extinction spectra, dark-field scattering, and response in electrical and optical fields. This material is available free of charge via the Internet at http://pubs.acs.org.

■ AUTHOR INFORMATION

Corresponding Author

*E-mail: ivan.smalyukh@colorado.edu.

Author Contributions

Q.L., Y.Y., and I.I.S. performed experimental work and analyzed results. Q.L. and Y.Y. synthesized nanoparticles. Q.L. developed the nanoparticle dispersion method. Q.L. and I.I.S. developed the physical model and wrote the manuscript. I.I.S. conceived and designed the project.

Notes

The authors declare no competing financial interest.

■ ACKNOWLEDGMENTS

■ REFERENCES

(1) Chaikin, P. M.; Lubensky, T. C. *Principles of Condensed Matter Physics*; Cambridge Univ. Press: Cambridge, 2000.

(2) Whitesides, G. M.; Grzybowski, B. *Science* **2002**, *295*, 2418−2421.

(3) Semonin, O. E.; Luther, J. M.; Choi, S.; Chen, H.-Y.; Gao, J.; Nozik, A. J.; Beard, M. C. *Science* **2011**, *334*, 1530−1533.

(4) Mertelj, A.; Lisjak, D.; Drofenik, M.; Čopič, M. *Nature* **2013**, *504*, 237−241.

(5) Liu, Q.; Senyuk, B.; Tang, J.; Lee, T.; Qian, J.; He, S.; Smalyukh, I. I. *Phys. Rev. Lett.* **2012**, *109*, 088301.

(6) Wood, T. A.; Lintuvuori, J. S.; Schofield, A. B.; Marenduzzo, D.; Poon, W. C. K. *Science* **2011**, *334*, 79−83.

(7) Lapointe, C. P.; Mason, T. G.; Smalyukh, I. I. *Science* **2009**, *326*, 1083−1086.

(8) Senyuk, B.; Liu, Q.; He, S.; Kamien, R. D.; Kusner, R. B.; Lubensky, T. C.; Smalyukh, I. I. *Nature* **2013**, *493*, 200−205.

(9) Poulin, P.; Stark, H.; Lubensky, T. C.; Weitz, D. A. *Science* **1997**, *275*, 1770−1773.

(10) Hsu, C. W.; Zhen, B.; Qiu, W.; Shapira, O.; DeLacy, B. G.; Joannopoulos, J. D.; Soljačić, M. *Nat. Commun.* **2014**, *5*, 3152.

(11) Smalyukh, I. I.; Shiyanovskii, S. V.; Lavrentovich, O. D. *Chem. Phys. Lett.* **2001**, *336*, 88−96.

(12) Bahadur, B. *Handbook of Liquid Crystals*; Wiley-VCH: Weinheim, 1998; Vol. 2A.

(13) Heilmeier, G. H.; Zanoni, L. A. *Appl. Phys. Lett.* **1968**, *13*, 91−92.

(14) Perez-Juste, J.; Liz-Marzan, L. M.; Carnie, S.; Chan, D.Y. C.; Mulvaney, P. *Adv. Funct. Mater.* **2004**, *14*, 571−579.

(15) Ye, X.; Zheng, C.; Chen, J.; Gao, Y.; Murray, C. B. *Nano Lett.* **2013**, *13*, 765−771.

(16) Aherne, D.; Gara, M.; Kelly, J. M.; Gun'ko, Y. K. *Adv. Funct. Mater.* **2010**, *20*, 1329−1338.

(17) Ramdane, O. O.; Auroy, P.; Forget, S.; Raspaud, E.; Martinot-Lagarde, P.; Dozov, I. *Phys. Rev. Lett.* **2000**, *84*, 3871−3874.

(18) von Maltzahn, G.; Centrone, A.; Park, J.-H.; Ramanathan, R.; Sailor, M. J.; Hatton, T. A.; Bhatia, S. N. *Adv. Mater.* **2009**, *21*, 3175−3180.

(19) Gardner, D. F.; Evans, J. S.; Smalyukh, I. I. *Mol. Cryst. Liq. Cryst.* **2011**, *545*, 1227−1245.

(20) Luk, Y.-Y.; Abbott, N. L. *Science* **2003**, *301*, 623−626.

(21) De Sio, L.; Serak, S.; Tabiryan, N.; Umeton, C. *J. Mater. Chem. C* **2013**, *1*, 7483−7487.

(22) Martinez, A.; Mireles, H. C.; Smalyukh, I. I. *Proc. Natl. Acad. Sci. U.S.A.* **2011**, *108*, 20891−20896.

(23) Zijlstra, P.; van Stee, M.; Verhart, N.; Gu, Z.; Orrit, M. *Phys. Chem. Chem. Phys.* **2012**, *14*, 4584−4588.

(24) Golovin, A. B.; Lavrentovich, O. D. *Appl. Phys. Lett.* **2009**, *95*, 254104.

(25) Zheng, X.; Fontana, J.; Pevnyi, M.; Ignatenko, M.; Wang, S.; Vaia, R.; Palffy-Muhoray, P. *J. Mater. Sci.* **2012**, *47*, 4914−4920.

(26) Blinov, L. M.; Cigrinov, V. G. *Electrooptic Effects in Liquid Crystal Materials*; Springer-Verlag: New York, 1996.

(27) Madhusudana, N. V.; Pratibha, R. *Mol. Cryst. Liq. Cryst. Lett.* **1982**, *89*, 249−257.

(28) Skarp, K.; Lagerwall, S. T.; Stebler, B. *Mol. Cryst. Liq. Cryst.* **1980**, *60*, 215−236.

(29) Kelly, K.; Coronado, E.; Zhao, L. L.; Schatz, G. C. *J. Phys. Chem. B* **2003**, *107*, 668−677.

(30) Kruk, G.; Kocot, A.; Wrzalik, R.; Vij, J. K.; Karthaus, O.; Ringsdorf, H. *Liq. Cryst.* **1993**, *14*, 807−819.

(31) Koenig, G. M.; de Pablo, J. J.; Abbott, N. L. *Langmuir* **2009**, *25*, 13318−13321.

(32) van der Schoot, P.; Popa-Nita, V.; Kralj, S. *J. Phys. Chem. B* **2008**, *112*, 4512−4518.

(33) Liu, Q.; Tang, J.; Zhang, Y.; Martinez, A.; Wang, S.; He, S.; White, T. J.; Smalyukh, I. I. *Phys. Rev. E* **2014**, *89*, 052505.